Synthetic Metals 209 (2015) 583–587

Contents lists available at ScienceDirect

Synthetic Metals

journal homepage: www.elsevier.com/locate/synmet

Short communication

Combined high permittivity and high electrical conductivity of carbon nano-onion/polyaniline composites

Anthony N. Papathanassiou[a,*], Marta E. Plonska-Brzezinska[b], Olena Mykhailiv[b], Luis Echegoyen[c,*], Ilias Sakellis[a]

[a] University of Athens, Physics Department, Solid State Physics Section, Panepistimiopolis, GR, 15784 Athens, Greece
[b] University of Bialystok, Institute of Chemistry, Hurtowa 1, 15-399 Bialystok, Poland
[c] University of Texas at El Paso, Department of Chemistry, 500 W. University Ave., El Paso, TX 79968 USA

ARTICLE INFO

Article history:
Received 13 June 2015
Received in revised form 10 August 2015
Accepted 19 August 2015

PACS indexes:
81.05.ub
77.84.Lf
72.80.Le
77.22.Gm

Keywords:
Carbon nano-onions
Polyaniline
Composites
Dielectric permittivity
Dielectric relaxation

ABSTRACT

We report high dielectric permittivity values for electrically conducting carbon nano-onion/polyaniline (CNO/PANI) composites. Broadband Dielectric Spectroscopy (BDS) measurements conducted under isothermal conditions from 16 K to room temperature in the frequency range between 1 mHz and 1 MHz, revealed a Cole–Cole relaxation mechanism. The intensity of the relaxation is comparable with the observed huge static dielectric constant values, and indicates a correlation between the intense capacitance effects and the relaxation. The relaxation dynamics involve single or two phonon assisted tunneling of the relaxing electric charge carriers (protons and electrons) at low temperatures, which transition to multi-phonon assisted tunneling relaxation above 100 K. Within the Mott–Davis model describing phonon-assisted tunneling relaxation in disordered media, the typical spatial scale relaxation occurs and is found to correlate with the size of the CNOs. The capacitance correlates with the large effective CNO surface areas.

The spherical and concentric graphene layers that constitute the carbon nano-onions, CNOs, provide high effective surface areas, when compared with other allotropes of carbons, such as carbon nanotubes, graphene, graphite etc. [1,2]. In principle, percolation of electric charge competes with trapping. CNO and conducting polymer (CP) composites are highly conducting due to the conjugated bond structures of the CPs and the intrinsic electronic properties of the CNOs. Nevertheless, the structural and electrical heterogeneity of the CNO/CP composites are expected to yield high static dielectric constant values, i.e., static dielectric permittivity. The present work addresses the capacitive nature of a good conductor at a microscopic level. The dual nature of composites is important for their further applications, such as for electrode materials for energy storage supercapacitors and for biocompatible electrodes. For technological applications, high capacitance results in significant charge storage, while a conductivity percolation network provides effective charge transfer. Alternatively, water-dispersed composites may form materials with hydrophilic hydrogels, yielding soft biocompatible electrodes that are compatible with tissues or organs in order to emit or collect electric signals (charge flow) stemming from biological processes.

The procedures for the functionalization of CNOs with phenyleneamine-terminated groups have been already reported in previous studies [3,4]. To introduce functional groups onto the CNO surfaces, the carbon nanostructures were treated with 4-aminobenzoic acid (4-ABAc). The reaction led to a pronounced increase of the dispersibility of the carbon nanostructures in protic solvents, and induced further polymerization of aniline to obtain CNOs/PANI [3]. The carbon nano-onion structures with very homogeneous layers of polyaniline can be clearly seen using TEM at high magnification (Fig. 1a). The diameters of the CNO/PANI particles are between 8 and 20 nm. The results of the SEM studies of CNOs and of the polyaniline composites on a gold foil are shown in Fig. 1b–d. The morphology of each modification step of the CNO surfaces differs from that of the films formed by non-functionalized nanostructures (Fig. 1b). The non-modified CNO particles formed spherical aggregates with diameter sizes between 5 and 20 μm. Oxidation of the CNO particles with 4-ABAc (Fig. 1c) formed

* Corresponding authors.
E-mail addresses: antpapa@phys.uoa.gr (A.N. Papathanassiou), echegoyen@utep.edu (L. Echegoyen).

http://dx.doi.org/10.1016/j.synthmet.2015.08.020
0379-6779/

more uniform and homogenous structures (aggregates approximately 1–3 μm in size). Further modification of the oxidized CNOs resulted in surface films (Fig. 1d), indicating that the composites exhibit a more porous structure, which should enable a more efficient accumulation of charge.

The scope of the present work was to investigate the interplay between high capacitance and high electrical conductivity of the CNO/PANI composites and prove the hypothesis that the large static dielectric permittivity value is related to the polarization (and charge storage) linked to the CNOs. The dynamics of electric charge flow from 16 K to room temperature provides information of the dynamics of electric charge carriers at a microscopic scale. Broadband Dielectric Spectroscopy (BDS) can simultaneously probe the dc and ac conductivity originating from the localized motion of electric charges and charge trapping (capacitance effects). Making measurements over a broad frequency range, different time and over spatial scales can provide long scale charge transfer properties along the volume of the specimen down to the nano-scale. Therefore, the spatiotemporal nature of BDS can probe the conduction percolation network of a material, as well as charge localization or immobilization due to its structural and electrical heterogeneity [6,7]. BDS measurements of onion-like structure/non-conductive polymer composites have already been published [8].

The CNO/PANI composites were compressed using an IR press to form disk shaped pellets of 4 mm diameter and 0.4 mm thickness. The small dimensions of the sample avoid having to silver-paste the two parallel surfaces in order to obtain Ohmic contacts. Instead, two thin indium foils were mechanically attached and squeezed on the parallel surfaces (comparative BDS scans at room temperature were done with various electrode materials such as bronze, gold, platinum etc. to test electrode effects); indium, being a soft metal, can make good contact with the specimens surfaces. The indium–specimen–indium 'sandwich' was placed in a capacitor type sample holder of a high-vacuum liquid helium cryostat (ROK, Leybold–Hereaeus) operating from 15 K to room temperature. A LTC 60 temperature controller was used to stabilize the temperature with an accuracy of 0.01 K. Complex permittivity measurements were performed in the frequency range between 1 mHz and 1 MHz with a Solartron SI 1260 Gain-Phase Frequency Response Analyzer, and a Broadband Dielectric Converter (Novocontrol). The data acquisition system was monitored by the WinDeta (Novocontrol) software.

The films were imaged by secondary electron SEM with the use of an S-3000N scanning electron microscope from FEI (Tokyo, Japan). The accelerating voltage of the electron beam was 20 keV. Transmission electron microscopic (TEM) images were recorded using the FEI Tecnai^{TM} G2 20 X-TWIN instrument. The accelerating voltage of the electron beam was 200 keV, the TEM point resolution was 0.25 nm, the TEM line resolution was 0.144 nm, the maximum diffraction angle was ±12°, and the working distance was 10 mm.

The real and imaginary components of the complex dielectric permittivity ε^* are related to the reversibly stored energy (capacitance effects) and the dissipated energy, respectively, during one cycle of the externally applied harmonic field of frequency f. Isotherms of Im(ε^*) and $Re(\varepsilon^*)$ vs. f are presented in Fig. 2. The low frequency region of $Re(\varepsilon^*)$ provides an estimate for the value of the relative static dielectric constant ε_s using the

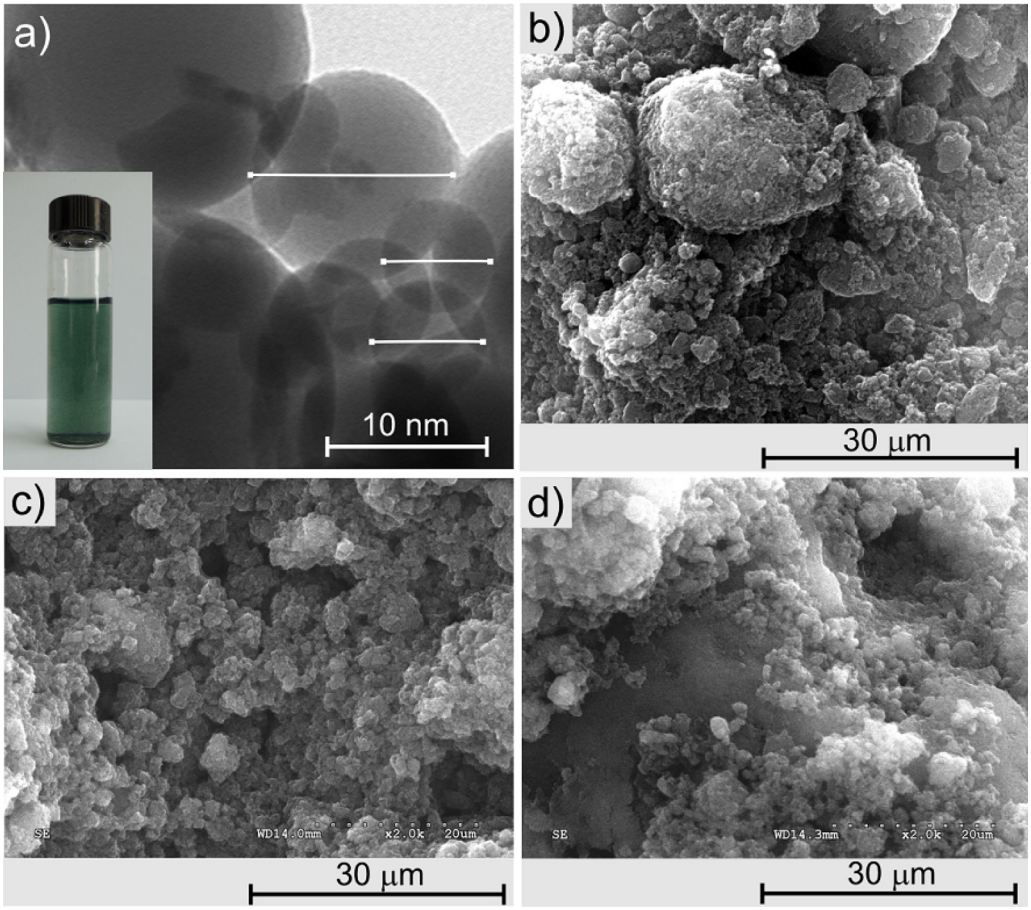

Fig. 1. (a) TEM images of CNOs/PANI, insert: the samples in 0.1 M HCl; (b–d) SEM images of the gold foil covered with (b) pristine CNOs, (c) oxidized-CNOs, and (d) CNOs/PANI.

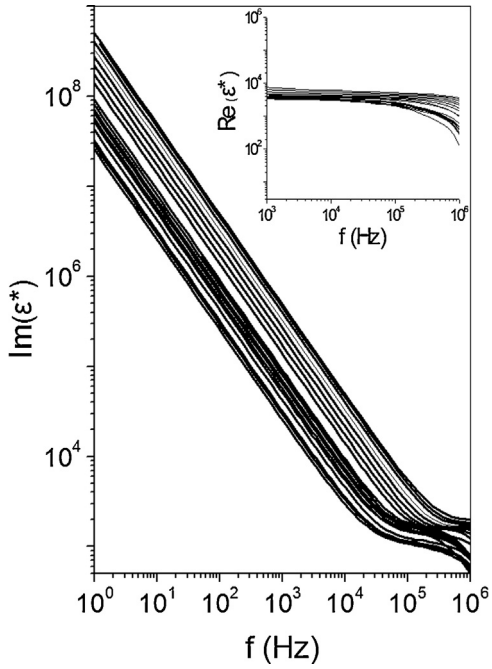

Fig. 2. Isotherms of Im(ε^*) vs. f of CNO/PANI composites from room temperature to 16 K (upper to lower curve, respectively). Inset: $Re(\varepsilon^*)$ vs. f isotherms.

relation $\varepsilon_s = \lim_{f\to 0}[Re(\varepsilon*)]$, which was found to be very large, ranging from roughly 6800 at room temperature to about 3250 at 16 K. While the nanocomposite is highly conducting, it simultaneously exhibits high capacitive properties. Giant dielectric constants can be observed in insulators, but are typically not observed for good electrical conductors. Generally, electric charges can either easily percolate or get trapped and thus, conductivity typically competes with capacitive effects. However, the static dielectric constant includes different components, such as electronic and atomic polarization, permanent electric dipole rotation, interfacial polarization etc. Therefore, it is necessary to resolve these components (typically, BDS detects such contributions as peaks in the relaxation spectra) and find those that contribute significantly to the large value of the static capacitance. The problem when performing BDS with conducting materials is that the dc-conductivity is high enough to mask the relaxation peaks. To overcome this problem, BDS isotherms are recorded at temperatures much lower than room temperature at which the dc-conductivity component is strongly suppressed and the dielectric relaxation peaks are more clearly revealed in the Im(ε^*) vs. f representation [7], since the dc-conductivity depends much more strongly on temperature than the intensity of the relaxation peaks. We observed that BDS isotherms from 16 K to room temperature for reference specimens of PANI did not show any relaxation peaks, while the static dielectric constant values were found to be an order of magnitude lower than those of CNO/PANI.

Isotherms of Im(ε^*) vs. f (Fig. 2) are typically fitted by the function:

$$Im(\varepsilon*) = \frac{\sigma_0}{\varepsilon_0 2\pi f^n} + \frac{\Delta\varepsilon}{\left(1+(f/f_0)^a\right)^b} \quad (1)$$

where σ_0 is the dc-conductivity, ε_0 is the permittivity of free space, $\Delta\varepsilon$ is the intensity of the relaxation mechanism, a and b are fractional exponents and f_0 is a parameter that coincides with the peak maximum frequency for $b = 1$. The first term represents a general fractional dc-conductivity with $0 < n \leq 1$ and the second is a Harviliak–Negami (HN) relaxation peak [9], where a $(0 < a \leq 1)$ and b $(0 < b \leq 1)$ are symmetric and unsymmetrical broadening parameters, respectively. For a Debye peak, the parameters amount to unity ($a = b = 1$). For the isotherms depicted in Fig. 2, that correspond to high temperature measurements, the dc-conductivity term is so intense that it masks any underlying relaxation that may exist. By reducing the temperature, σ_0 is suppressed, and the relaxation processes are revealed at the high frequency limit, which gradually shifts toward lower frequencies. For temperatures lower than 200 K, the maxima for the relaxation peaks can be observed gradually within the working frequency region (i.e., below 1 MHz). Eq. (1) perfectly fits the experimental data (Fig. 3). For the entire set of temperatures, the values of the conductivity exponent n are about 0.2% less than unity indicating that at the low frequencies the conductivity is practically constant. Below 200 K the value of the unsymmetrical-broadening parameter b was found to be equal to unity, implying that the relaxation time values are distributed symmetrically around f_0^{-1} (Cole–Cole (CC) distribution) [10].

A Stickel plot relates the logarithmic frequency versus the reciprocal temperature and is used to identify the dynamic crossover from one mode of relaxation to another [11]. In a Stickel plot for the peak maximum the data points can be fitted by two straight lines (Fig. 4). In the low temperature regime, the apparent activation energy (defined as $E \equiv -d\ln f_0/d(1kT)$, where k denotes Boltzmann's constant) was found to be extremely small ($E = (0.3 \pm 0.1)$meV). Above 100 K, the data points lie on a straight line, which yields activation energy $E = (28 \pm 2)$meV, which is two orders of magnitude higher than that observed for the low temperature region. The phonon-assisted tunneling of electric charges (protons) within a double potential is theoretically well understood [12]. The electric charge carriers in conducting polyaniline are mainly protons that are mainly located at the redox centers close to the nitrogen atoms of the polyaniline backbone that distort neighboring bonds and form a polaron. Generally, we can conclude that the type of electric charge flow is mainly electronic, based on the protons and electrons of the CNOs. One-phonon assisted tunneling predicts $f_0 \propto \coth(\Delta/kT)$, where Δ is the asymmetry energy; given that Δ is dramatically smaller than

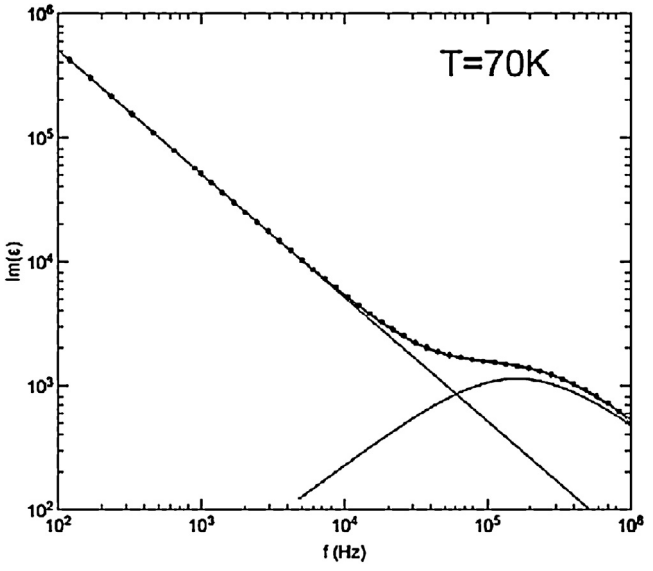

Fig. 3. Im(ε^*) vs. f data points collected at 70 K. Eq. (1) was fitted to the data points (the underlying straight line and relaxation peak are the constituents of the fitted curve). Fitting results: $\log\sigma_0 = (-4.552 \pm 0.002)$ (σ_0 in S/cm), $n = 0.9979 \pm 0.0005$, $\log f_0 = 5.204 \pm 0.005$ (f_0 in Hz), $\Delta\varepsilon = 2760 \pm 20$, $a = 0.876 \pm 0.006$, $b = 1$. The latter value indicates a symmetric distribution function around $\log f_0$, according to the Cole–Cole model.

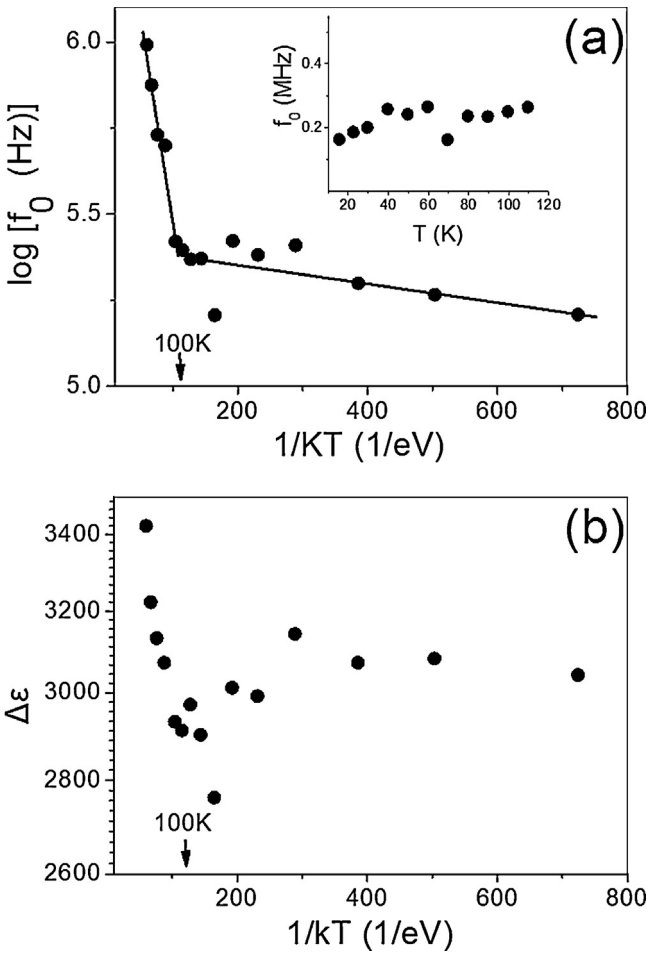

Fig. 4. Stickel plots for f_0 (a) and $\Delta\varepsilon$ (b), respectively. At 100 K there is a change in the relaxation dynamics, which is interpreted from multi-phonon tunneling to single or double phonon assisted tunneling relaxation as the temperature is decreased. Inset of (a): f_0 vs. T dependence for the low temperature region of a Stickel plot.

the potential barrier height, f_0 varies slightly with temperature [13]. One-phonon assisted tunneling through a barrier separating a pair potential alternatively predicts, a linear dependence of f_0 and T [14]. A more general treatment predicts a linear dependence of f_0 with temperature, in the low temperature limit, and an Arrhenius temperature dependence at higher temperatures, where multi-phonon assisted tunneling occurs [16]. As can be seen in the inset of Fig. 4, a slight increase of f_0 vs. T occurs, indicating a one-phonon assisted tunneling process [13] that explains the low-temperature dynamic behavior [14]. At higher temperatures, the Arrhenius behavior is attributed to multi-phonon assisted tunneling, in accordance with a hopping theory [16]. The intensity $\Delta\varepsilon$, when plotted against the reciprocal temperature, supports the dynamic transition revealed from the Stickel plot for the relaxation maximum f_0 (Fig. 4b).

The low temperature values of the static dielectric constants, reported in this work are comparable to the $\Delta\varepsilon$ values of the recorded dielectric relaxation peaks; i.e., the major contribution to the observed static dielectric constant stems from the observed high-frequency dielectric relaxation mechanism. The high temperature dielectric relaxation time τ of an electron (or proton) relaxing between two localized states at a distance R by multi-phonon assisted tunneling through the intermediate potential barrier, can be found from the Mott–Davis equation [16]:

$$\tau = \nu_{ph}^{-1} \exp(2\alpha R) \exp\left(\frac{E}{kT}\right) \quad (3)$$

where ν_{ph} is a vibrational frequency (roughly equal to a phonon frequency), α is the inverse localization length of the electron's wave-function and E is an effective activation energy. As mentioned above, the high temperature data points presented in Fig. 4 can be fitted to an Arrhenius law $f_0 = C \exp(-E/kT)$, which together with Eq. (3) (since $\tau \equiv f_0^{-1}$) yields [18]:

$$R = (2\alpha)^{-1} \ln\left(\frac{\nu_{ph}}{C}\right) \quad (4)$$

By fitting a straight line to the high temperature relaxation data depicted in Fig. 4, we calculated $E = (0.3 \pm 0.1)$ meV and $\ln C = (15.4 \pm 0.2)$ (C in Hz). Protons are mostly localized at redox centers close to the nitrogen atoms on the polyaniline backbone. The wave function of pinned polarons (which contribute to polarization, but not to the dc-conductivity) is localized at distances comparable to the dimensions of one aniline ring. Therefore, the localization length should be about $\alpha^{-1} = 6.9$ A° [19]. Typical phonon frequency values for conducting polymers are $\nu_{ph} \sim 10 - 40$THz and using Eq. (3) we determined $R \sim 5.0 - 5.1$ nm. The latter value is the typical spatial scale for dielectric relaxation and for the high static dielectric constant. Its value is comparable to the diameter of the CNO nanostructures, which means that the observed intense polarization phenomena are related to the CNOs. While the presence of the CNO nanostructures increase the total effective conductivity of the composite, they also contribute to the structural and electrical heterogeneity of the composite to result in enhanced capacitance effects.

The CNO/PANI composites exhibit large static permittivity values and high electrical conductivity, compared with those of a reference PANI specimen. Simultaneously BDS studies between 16 K and room temperature trace an intense relaxation peak, which is absent is comparative studies at a reference PANI sample. It seems likely that the large static permittivity values and the presence of the intense relaxation are related to the presence of CNOs in the composite material. Subsequent analyses of the experimental data showed that the huge static permittivity is related to a dielectric relaxation mechanism below 1 MHz, which involves spatial scales for relaxation comparable to the diameters of the CNOs. The high static permittivity is probably related with the large surface of CNOs. The nanocomposites can therefore store charge and at the same time transfer it when used as electrode materials for electric double layer ultracapacitors. Alternatively, the combination of high dielectric permittivity and high electrical conductivity translate to good device performance. Moreover, its good dispersibility in protic solvents makes the CNO/PANI composites suitable for biocompatible electrode applications.

Acknowledgments

We gratefully acknowledge the financial support of the National Science Centre, Poland, and grant #2012/05/E/ST5/03800 to M.E.P.-B. L.E. thanks the Robert A. Welch Foundation for an endowed chair, grant #AH-0033 and the US NSF, grants: DMR-1205302 (PREM Program) and CHE-1408865.

References

[1] D. Ugarte, Nature 359 (707) (1992) .
[2] J.L. Delgado, M.A. Herranza, N. Martin, J. Mater. Chem. 18 (1417) (2008) .
[3] M.E. Plonska-Brzezinska, J. Mazurczyk, B. Palys, J. Breczko, A. Lapinski, A.T. Dubis, L. Echegoyen, Chem. Eur. J. 18 (2600) (2012) .

[4] H. Zengin, W. Zhou, J. Jin, R. Czerw Jr., D.W. Smith, L. Echegoyen, D.L. Caroll, S.H. Foulger, J. Ballato, Adv. Mater. 14 (1480) (2002) .
[6] A.N. Papathanassiou, I. Sakellis, J. Grammatikakis, Appl. Phys. Lett. 91 (122911) (2007) .
[7] A.N. Papathanassiou, I. Sakellis, J. Grammatikakis, E. Vitoratos, S. Sakkopoulos, Appl. Phys. Lett. 103 (123304) (2013) .
[8] J. Macutkevic, I. Kranauskaite, J. Banys, S. Moseenkov, V. Kuznetsov, O. Shenderova, J. Appl. Phys. 115 (2014) 213702.
[9] S. Havriliak, S. Negami, J. Pol. Sci. C 14 (89) (1966) .
[10] R.H. Cole, K.S. Cole, J. Chem. Phys. 9 (341) (1941) .
[11] F. Stickel, E.W. Fischer, R. Richert, J. Chem. Phys. 102 (6251) (1995) .
[12] I. Kuskovsky, B.S. Lim, A.S. Nowick, Phys. Rev. B 60 (1999) R3713.
[13] Bottger, V. Bryskin, Hopping Conduction in Solids, Akademie Verlag, Berlin, 1985 Chapter IV.
[14] I.A. Sussmann, Phys. Kondens. Mater. 2 (146) (1964) .
[16] M.P. Tonkonogov, V.Y. Medvedev, Soviet Phys. J. 30 (122) (1987) .
[18] A.N. Papathanassiou, I. Sakellis, J. Grammatikakis, S. Vitoratos, E. Sakkopoulos, Solid State Commun. 125 (2003) 95.
[19] J.M. Ginder, A.J. Epstein, Phys. Rev. B 41 (10674) (1990) .